2023

Understanding the Mechanisms by which Cable Sway Produces Motion Artifact in Mobile Electroencephalography

David Rojas
University of Central Florida

UNDERSTANDING THE MECHANISMS BY WHICH CABLE SWAY PRODUCES MOTION ARTIFACT IN MOBILE ELECTROENCEPHALOGRAPHY

by

DAVID SEBASTIAN ROJAS
B.S. University of Florida, 2019

A thesis submitted in partial fulfillment of the requirements
for the degree of Master of Science
in the Department of Mechanical and Aerospace Engineering
in the College of Engineering and Computer Science
at the University of Central Florida
Orlando, Florida

Summer Term
2023

ABSTRACT

Mobile brain/body imaging utilizes electroencephalography (EEG) to record brain activity during human walking in dynamic environments. Motion artifact from cable sway affects the quality of EEG signals collected from the scalp, masking contributions of synchronously firing neurons. Previous studies have explored cable sway-induced motion artifact, but only during vigorous exercise or controlled sinusoidal motion. Therefore, a need remains to further understand the underlying mechanisms of this artifact, as it may help with developing real-time mitigation methods, reducing reliance on offline signal processing. In this thesis, I aimed to show that controlled cable sway could produce specific motion artifact waveforms in a benchtop setup. I programmed a robotic arm to perform three different types of waveform motions - sinusoidal, square, and sawtooth - in two setups that had different levels of cable support: constrained and unconstrained. I used a novel dual-sided EEG electrode where one side of the electrode interfaces with the scalp to record traditional EEG signals while an outer-facing electrode interfaces with a conductive fabric cap to record isolated motion artifact and noise. Additionally, I placed the electrodes in a 3D-printed holder designed to position them between two layers of conductive fabric and eliminate any electrode movement, which has not been previously constrained. Lastly, I computed correlations between cable sway and bottom electrode EEG, cable sway and top electrode EEG, and top and bottom EEG. Correlations for all variable combinations were low, ranging from -0.122 +/- 0.223 to 0.058 +/- 0.238. Out of six correlation measure comparisons (three across testing setups and three across waveform motions), five did not show significant differences (p-values = 0.391 - 0.958). These results suggest that EEG motion artifact is not the

result of just mechanical deformation of the cables but likely requires simultaneous movement of the electrode itself, altering the electrode-conductive surface interface dynamics.

ACKNOWLEDGEMENTS

First and foremost, I would like to express my greatest appreciation for my advisor, Dr. Helen J. Huang, for her endless patience and continuous guidance from the beginning to end of this project. While moving forward through my thesis, I never expected that I would have to make some difficult decisions or that I would have to ask myself some tough questions that I have previously tried to avoid, but Dr. Huang's encouragement and insightful feedback made me recognize how much these decisions and questions were necessary for my development as a professional.

Additionally, I would like to extend my thanks to my thesis committee members, Dr. Luigi Perotti and Dr. Qiushi Fu, for their feedback and suggestions, the former of which gave me a greater sense of confidence in my comprehension of the research topic I chose, my presentation skills, and my ability to convey information through detailed visuals, and the latter of which encouraged me to think about how to expand my work beyond what I had already done and approach my findings from different angles.

Furthermore, I would like to thank Dr. Jinfeng Li for providing me all the technical knowledge I needed to use the equipment that would come into play during my data collection, as well as for helping me in a few times of crisis where I had to troubleshoot problems affecting my testing setups. His willingness to explain or clarify aspects of the conceptual framework relevant to my thesis that went beyond what I understood from reading relevant literature also allowed me to move forward in certain stages of my research where I felt stuck and confused.

I am also immensely grateful for my parents and my older brother for sometimes knowing me better than I know myself, reminding me that I have always had the ability to endure in the

face of adversity and accomplish remarkable personal, academic, and professional feats, even though I have always struggled with reminding myself.

Finally, and most importantly, I would like to thank my amazing girlfriend Gabriela and my adorable dogs, Charlotte and Hershey, for being my reason to push forward, work incredibly hard, and never give up, and simultaneously make sure to care for my physical and mental health, always prioritizing a healthy work-life balance. Gaby never stopped believing in me even when I felt like I no longer had the strength to do the same, and the vast goodness of her heart always made me feel heard, understood, sheltered, and at peace in times of extraordinary crisis along this journey. I love you more than words can capture.

TABLE OF CONTENTS

LIST OF FIGURES

CHAPTER 1: INTRODUCTION

Mobile brain/body imaging is an approach that combines several different data collection methods and stimulus inputs to evaluate the relationship between brain dynamics and whole-body movement (Jungnickel et al., 2019). One such data collection method is electroencephalography (EEG), which is a non-invasive technique for recording the electrical activity of the human brain that is widely used for clinical applications due to its exceptionally high temporal resolution (Casson et al., 2018). However, because the summated postsynaptic potentials from multitudes of synchronously firing neurons have a small magnitude, the resulting EEG signals are often masked by electrical activity from other sources external to the brain, such as other parts of the body or the environment. This interfering electrical activity creates distortions, or artifacts, in EEG recordings, making it difficult to accurately distinguish between neuropathological events and artifacts, as well as identify normal brain waves (Britton et al., 2016). These challenges are particularly unfavorable for studies that involve recording electrocortical brain dynamics during human locomotion, specifically walking. Because walking is such an important motor task for everyday life, understanding its underlying neural mechanisms and how they are associated with actions such as speeding up/slowing down, maintaining balance when perturbed, and staying clear of obstacles, is critical for defining the level of the brain's involvement throughout the gait cycle (Jacobsen et al., 2022). However, EEG data collected during walking is susceptible to a specific type of environmental artifact known as motion artifact, the potential sources of which include head movement and cable sway (Gwin et al., 2010; Oliveira et al., 2016).

Although previous studies have shown that head movement-related motion artifact is likely attributed to the motion of EEG electrodes with respect to the scalp, this issue has been partially

remedied by the use of active electrodes – EEG electrodes integrated with preamplifiers – in place of passive electrodes (Mihajlovic et al., 2014; Xu et al., 2017). Continuous monitoring of electrode-skin contact impedance as well as increased electrode surface area have also been shown to help with reducing this type of motion artifact (Bertrand et al., 2013; Symeonidou et al., 2018). Cable sway-induced motion artifact, on the other hand, is believed to be the result of triboelectric noise produced by the friction and mechanical deformation of the EEG cable insulators when the cables are subjected to movement during human locomotion (Simakov & Webster, 2010; Webster, 1984). Cable shielding combined with the use of active electrodes have been suggested to reduce this artifact (Mihajlovic et al., 2015). However, previous research by Symeonidou et al. (2018) has shown the limited effectiveness of this hardware approach through a benchtop evaluation of cable sway-induced motion artifact, in which controlled cable sway was produced using a motion platform that moved the shielded cables using a controlled sinusoidal motion, and EEG signals were recorded with flat-type active electrodes. The study outcomes revealed that the artifact still significantly affected the quality of the EEG signal, linearly decreasing the signal-to-noise ratio as the frequency of controlled cable sway increased.

Developed primarily as an advanced method of addressing motion artifact caused by head movement, dual-sided EEG electrodes offer potential as a more effective method of removing motion artifact caused by cable sway. In a dual-sided EEG electrode, the bottom electrode, which is a pin-type active electrode, has been shown to record electrocortical signals with accompanying motion artifacts, while the top electrode, which is an inverted flat-type active electrode, is electrically independent and has been shown to record motion artifact and electrical noise only. Because both electrodes are mechanically coupled to each other, they experience the same motion and capture similar levels of noise. Consequently, the noise characteristics in the isolated signal

from the top electrode closely resemble those in the scalp EEG signal from the bottom electrode. This facilitates artifact removal using sliding window spectral subtraction, as the frequency content of the noise in the scalp EEG signal can be directly extracted using a Fast Fourier Transform on each window of the isolated noise signal from the top electrode (Nordin et al., 2018). Utilizing this frequency information, a more reliable threshold for artifact cancellation can be defined, avoiding the need to derive it from an estimated noise spectrum. As a result, the quality of an EEG signal recorded during head movement can be effectively restored, minimizing the effects of motion artifact and electrical noise, to resemble signals recorded under stationary conditions. However, one study about this particular approach showed that the frequency spectra of the signal from the top electrode do not just capture the motion frequency of the head, but may also capture cable motion, though to a lesser extent compared to the former, which agrees with other studies related to motion artifact isolation and reduction through software or hardware approaches (Gwin et al., 2010; Kline et al., 2015; Nordin et al., 2018). The frequency components associated with head movement and the components associated with cable motion are likely both attenuated in the process of sliding window spectral subtraction, but the actual contributions of the components associated with cable motion are not completely understood because the dual-sided electrode setup used by Nordin et al. (2018) required the use of a secondary cap tightly overlaid on the top electrodes, thereby also holding the cables in the same location in place.

A different dual-sided electrode setup that does not require such tight contact between the top electrodes and the secondary cap, the latter of which forms a conductive interface with the top electrodes, can allow for improved visualization of the frequency components of the isolated motion artifact prior to artifact removal, such as one created for a study that investigated the relationship between the signals recorded by both the top and bottom electrodes. In this study, the

dual-sided electrode setup did not use a phantom head, and instead used a 3D-printed structure to hold two pieces of conductive stretch fabric parallel and close to each other, such that the bottom fabric piece served as the primary layer, in place of the primary cap, and the top fabric piece served as the secondary layer, in place of the secondary cap. In this configuration, the dual-sided electrodes were moved in a controlled manner by a user-operated robotic arm. The movements were produced with different combinations of displacement magnitude, frequency, and direction, and were tracked with motion capture as EEG signals were simultaneously collected. Signals from the top and bottom electrodes exhibited dominant frequencies closely corresponding to the movement frequencies of the electrodes themselves, reinforcing that the top side of a dual-sided electrode can effectively isolate the motion artifact produced by movement of the platform on which the electrodes sit (Li, 2022).

Therefore, given that previous research has suggested that dual-sided EEG electrodes are effective for 1) recording isolated head movement-induced motion artifact and 2) improving the outcome reliability of offline signal processing techniques like sliding window spectral subtraction and independent component analysis, using this novel hardware approach to record isolated cable sway-induced motion artifact may potentially be more effective for minimizing its effects on EEG signal quality and may even inform the development of real-time artifact reduction methods (Li, 2022; Nordin et al., 2018; Richer et al., 2020). However, it is first necessary to determine whether cable sway can produce motion artifacts that can be captured and isolated by dual-sided EEG electrodes, regardless of how the cables move. This may require expanding beyond the controlled cable sway produced by controlled sinusoidal motion in previous research and using other periodic motions to produce different variations of controlled cable sway.

The purpose of this thesis was to produce motion artifacts in dual-sided EEG resembling specific waveforms used to control cable sway. I used a custom electrode-conductive surface interface and a robotic arm with a cable holding attachment to record EEG signals under several different controlled cable sway conditions. These conditions involved performing the waveform motions with different levels of cable support. I hypothesized that 1) the signals recorded from both sides of a dual-sided EEG electrode would have a high correlation with each other across all waveform motions, 2) the signal from the top side of the electrode would have a high correlation with each type of waveform motion, 3) the signal from the bottom side of the electrode would have a high correlation with each type of waveform motion, and 4) less cable support during controlled motion, and thus more unconstrained cable sway, would result in lower values for these correlations compared to constrained cable sway from more cable support.

CHAPTER 2: METHODOLOGY

Testing Setup

I placed one dual-sided EEG electrode, a common mode sense (CMS) reference electrode, and a driven right leg (DRL) reference electrode in a 3D printed electrode holder. The electrode holder contained three wells: one for the CMS electrode, another for the DRL electrode, and a third for the dual-sided electrode, which from this point forward will be referred to as the C18 electrode in accordance with the identification and numbering system of the EEG ribbon cable strip that was used (Fig. 1A). The unused electrodes were bundled together in small drawstring nylon bags and bound to the cables to prevent them from behaving as a separate component with the potential to interfere with cable sway. A conductive fabric incorporated into the top and middle frames of the holder made contact with the top and bottom sides of the three electrodes (Fig. 1B). In contrast with the structure used by Li (2022), which served exclusively to house the conductive fabric while a separate structure was used to hold the electrodes as they were moved, allowing translation of the electrodes in different directions between the two layers, I designed the electrode holder to minimize electrode movement relative to the conductive fabric layers to control any impact of this movement on the EEG signal. I accomplished this by adding a static platform centered between the electrode wells in the middle frame of the structure with an electrode well incorporated into the platform. As an additional precaution against electrode movement, the electrode holder itself was fixed to a motionless, flat surface. The electrodes were connected to two analog-to-digital (AD) converter boxes connected to each other in a linear series (ActiveTwo, BioSemi B.V., Amsterdam, the Netherlands), allowing for the EEG signals from both sides of the electrode to be synchronously recorded at 512 Hz.

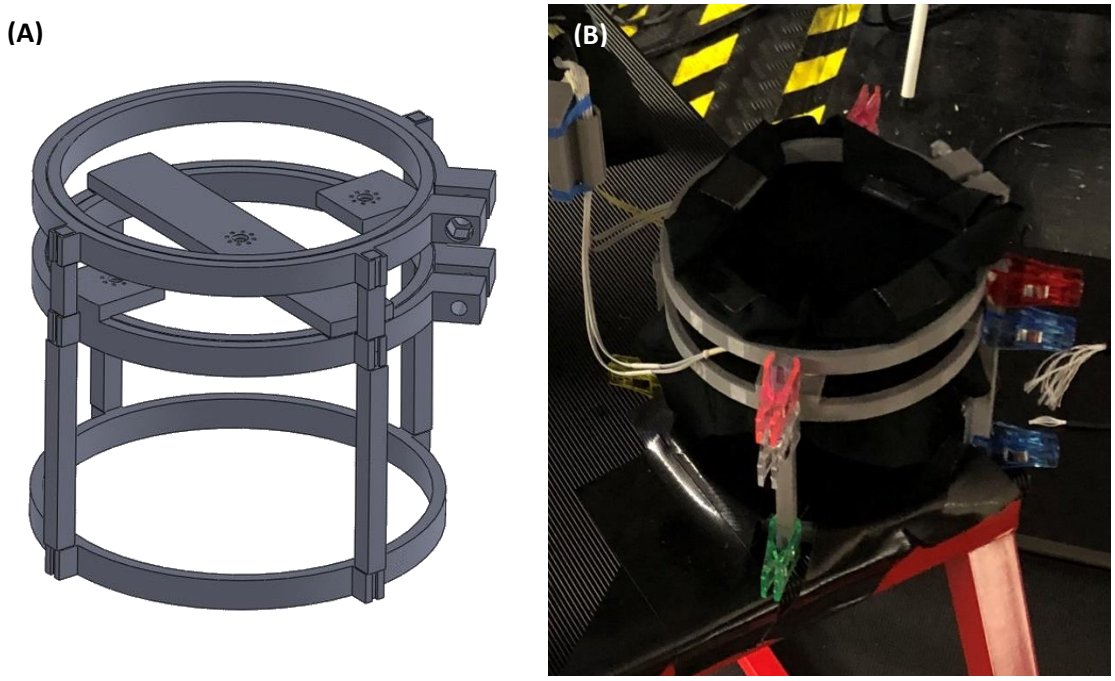

Figure 1: 3D-printed electrode holder. (A) An isometric view of the electrode holder's 3D structure. The bottom ring-like frame served as the base and was connected to the middle frame. The middle frame included three rigid, static platforms with electrode wells. The two wells on the sides were used to insert the CMS and DRL reference electrodes, while the center well was used to insert the C18 electrode. (B) The electrode holder with conductive fabric layers included. Bolts were used to fasten the middle and top frames to smaller, ring-like components, allowing the fabric pieces to be held in place and thereby creating an electrode-conductive surface interface.

To evaluate how constrained cable sway and unconstrained cable sway affect the generation of motion artifact, I assembled two benchtop testing setups with different levels of cable support. In the first testing setup, which from this point forward will be referred to as the Constrained setup, the cables were supported at three different points along their collective length. At the first point, which was located close to the elevated platform holding the AD converter boxes, I suspended the cables using a thin rope that I then tied to a metal bar behind the elevated platform. I created the second support point by laying the cables over a custom-designed rack fixed to a plyometric box. For the third point, I inserted the cables through a 3D printed cable holder attached to a desktop-grade robotic arm (DOBOT Magician Lite, Shenzhen Yuejiang Technology,

Shenzhen, China) placed on top of the same plyometric box as the custom-designed rack (Fig. 2). The cable configuration resulting from this level of physical support isolated controlled cable sway to only a short length of the cables situated between the cable holder and electrode holder. This was done to ensure that the robotic arm produced constrained sway in the cables. In the second testing setup, which from this point forward will be referred to as the Unconstrained setup, the cables were supported at only one point: the location where they were inserted in the cable holder. Additionally, I placed the robotic arm closer to the AD converter boxes, positioned it perpendicular to the orientation of the cables, removed the custom-designed rack, and fixed the electrode holder to a shorter plyometric box. The length of cables previously supported by the custom-designed rack was allowed to hang freely, resulting in the entire cable length having a J-shape due to the weight of the bound bundle of unused electrodes (Fig. 3). I expected that the cable configuration resulting from this limited physical support would allow unconstrained cable sway upstream of the electrodes when the robotic arm performed controlled motions at the support point.

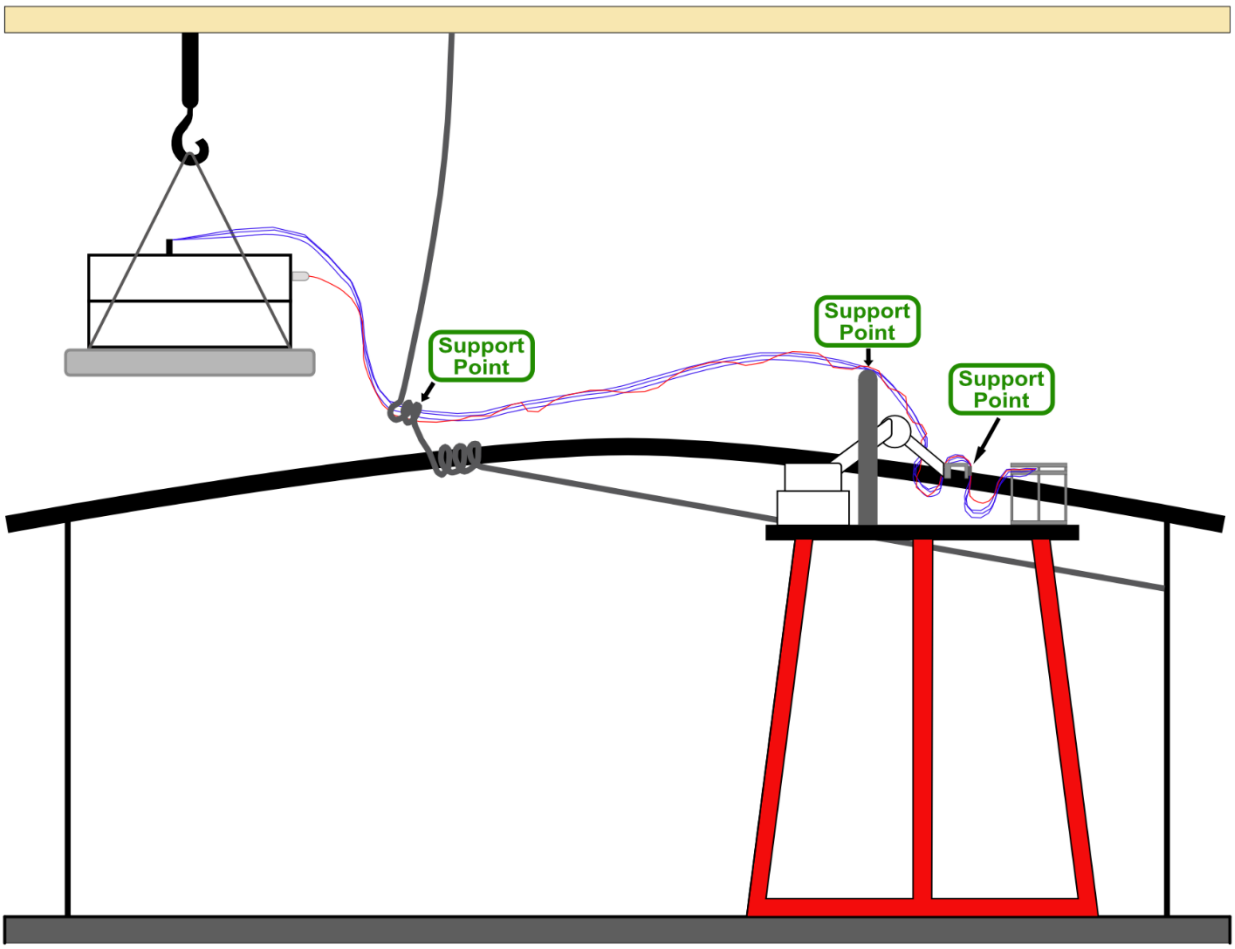

Figure 2: Schematic of the Constrained setup. The AD converter boxes were placed on an elevated platform suspended from the ceiling (upper left). The electrodes were connected to the electrode holder placed on a plyometric box (far right). The cables were inserted in the cable holder attached to the robotic arm (far right). The robotic arm was placed close to the electrode holder and the cables were supported at two additional points: the custom rack positioned over the robotic arm and the suspension provided by the thin rope.

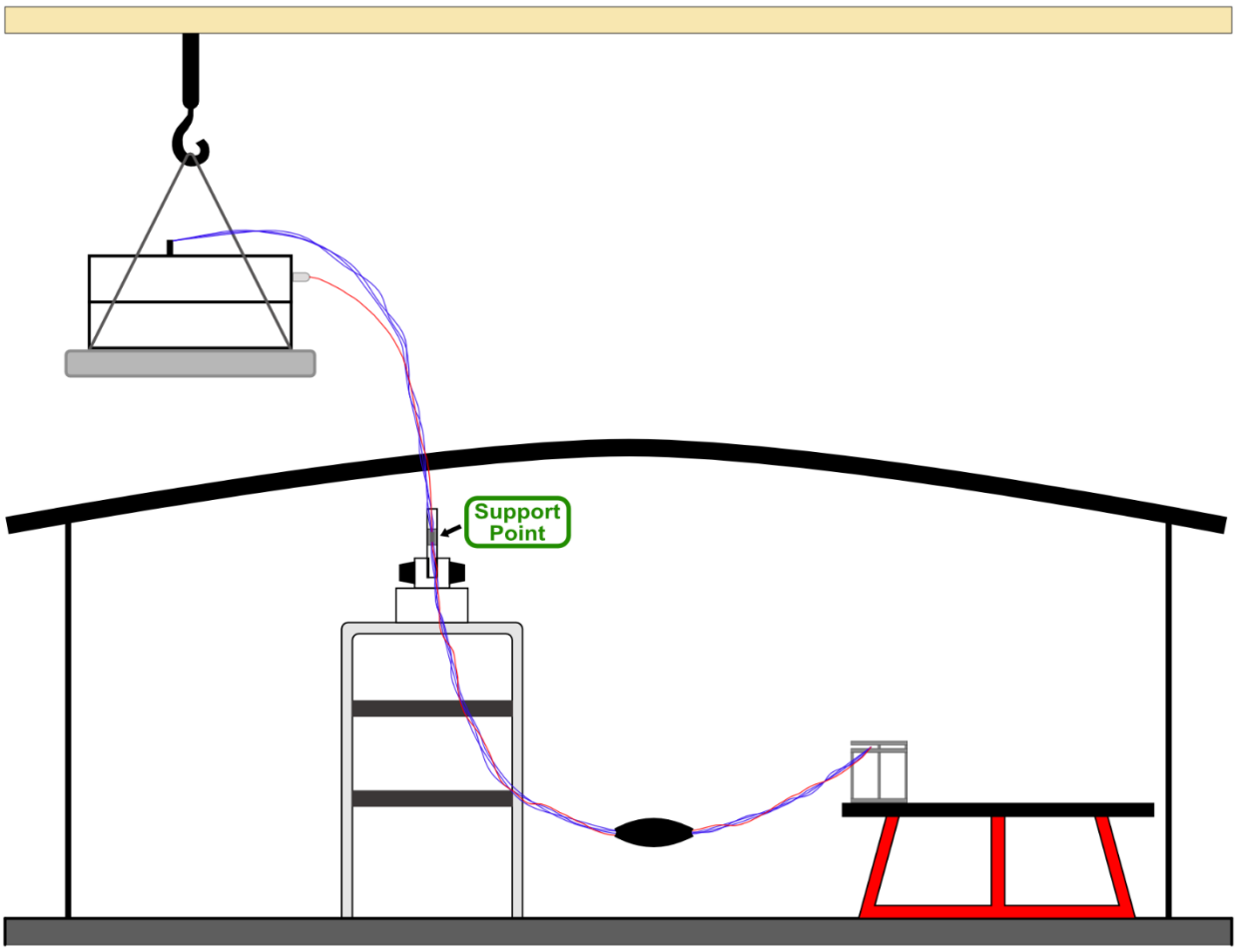

Figure 3: Schematic of the Unconstrained setup. The electrodes were connected to the electrode holder placed on a shorter plyometric box (far right). The robotic arm was placed closer to the AD converter boxes (left). The custom rack and thin rope were removed, allowing the cables to hang freely between the cable holder and the electrode holder. The dark, oval-shaped object represents the bound bundle of unused electrodes (lower middle).

For both testing setups, I programmed the robotic arm to move the cables with one of three controlled, periodic motions, each resembling a different waveform: sinusoidal, square, and sawtooth (Fig. 4). To track controlled cable sway, I attached three passive reflective markers on the top surface of the cable holder and recorded the marker movements using a motion capture system (OptiTrack, NaturalPoint Inc., Corvallis, OR, USA, 13 Prime13W cameras and 9 Prime13 cameras) with a sampling frequency of 240 Hz. The location on the cable holder that I selected for

marker placement was assumed to approximate the movement of the cables inserted in the cable holder. The robotic arm performed all waveform motions in a side-to-side direction perpendicular to the orientation of the cables (Fig. 2, Fig. 3).

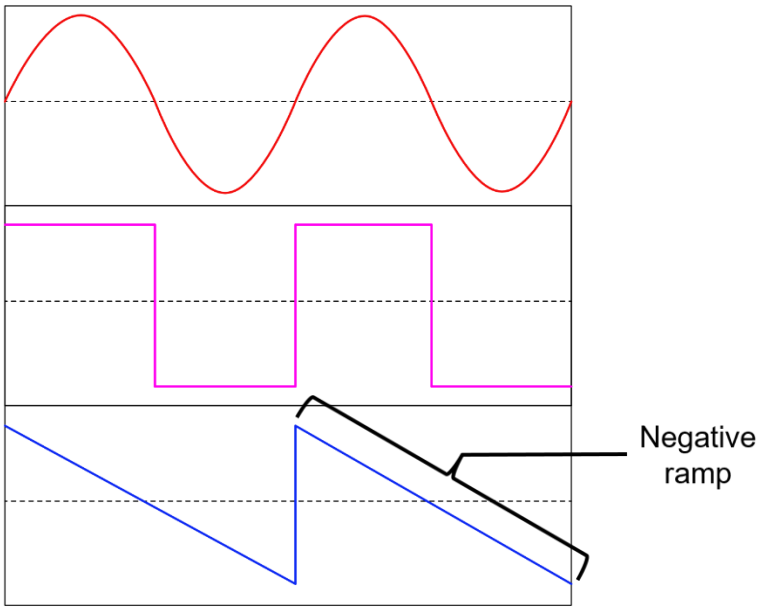

Figure 4: The different waveforms programmed into the robotic arm to move the cables with different controlled motions. From top to bottom, the sinusoidal, square, and sawtooth waveforms.

Protocol

I programmed the robotic arm to perform each waveform motion – sinusoidal, square, and sawtooth – with a displacement magnitude of 2 cm. The sinusoidal motion was performed with a frequency of 1 Hz, the square motion with a frequency of 0.5 Hz, and the sawtooth motion with a frequency of 0.5 Hz. All data were recorded in one day divided into two (2) experimental blocks: the first block in the Constrained setup, followed by the second block in the Unconstrained setup. Each block consisted of three (3) trials, one (1) trial for each of the waveform motions, in an order that was randomized (Fig. 5). A trial consisted of 60 movement cycles. For the duration of each

trial, I simultaneously recorded motion capture and collected EEG signals from both sides of the C18 electrode. With the completion of both blocks, I effectively completed two (2) trials for each waveform motion and three (3) trials for each testing setup. In total, I collected data for six (6) unique condition combinations.

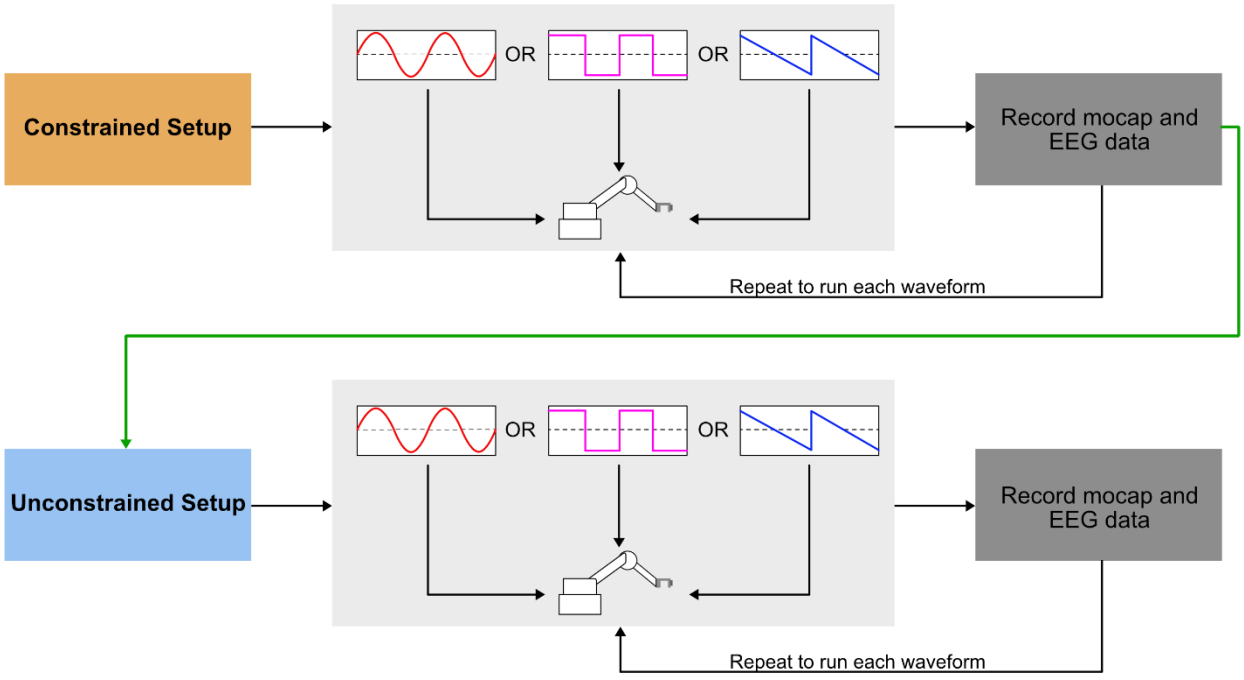

Figure 5: Flowchart summarizing the recording protocol. After completing the trials for the waveform motions, the Constrained setup was changed to the Unconstrained setup, as indicated by the green arrow, and the process was repeated. The order of the waveform motions was randomized for each block.

Data Analysis

All data were analyzed in MATLAB (version 9.11, R2021b, MathWorks Inc., Natick, MA, USA). Given the differences in shape and frequency between the waveform motions, I developed three different signal processing approaches for the motion capture marker tracking data and applied them based on the specific waveform motion during which the trial data was collected. For the sinusoidal motion, I low-pass filtered the tracking data using a fourth-order Butterworth

filter with a 12 Hz cutoff frequency. For the square motion, I low-pass filtered the tracking data using a sixth-order Butterworth filter with a 5 Hz cutoff frequency. Finally, for the sawtooth motion, I low-pass filtered the tracking data using a seventh-order Butterworth filter with a 5 Hz cutoff frequency. I then determined the start and end points of controlled cable sway as well as the start and end points of each movement cycle to visualize the 60 total movement cycles only. With this extracted data, I normalized the amplitude of cable sway by dividing the amplitudes of the 60 total movement cycles by the maximum peak-to-peak amplitude, and then used the middle 30 movement cycles for additional analyses (Li, 2022). Given their different scales and units, I performed normalization of both the motion capture marker tracking data and the EEG signal data to place them on the same scale, thereby making their ranges comparable and facilitating visual distinction of their different magnitudes (Javaheri et al., 2014; Singh & Singh, 2020).

Additionally, for each trial, I separated out the top and bottom electrode EEG, bandpass filtered each signal from 0.5 to 59 Hz and removed line noise. Similar to the normalization procedure for cable sway amplitude, for each separated signal, I normalized the amplitude by dividing it by the maximum peak-to-peak amplitude (Li, 2022). In each normalized signal, I identified when controlled cable sway started and ended by analyzing the event latency indicating when the motion capture recording started, using the EEG sampling rate to convert the cable sway start and end points in the respective marker tracking data to time points in the EEG signal data, and defining these time points relative to the motion capture recording start time. Subsequently, I determined the set of EEG data points that coincided with the middle 30 movement cycles and divided the set into 30 segments with lengths that matched the movement cycle lengths.

I used all three extracted data sets to calculate the correlation between 1) cable sway and EEG from the bottom electrode, 2) cable sway and EEG from the top electrode, and 3) EEG from

both the top and bottom electrodes for the given trial. I then performed the Fisher Z transformation on the correlation values (Li, 2022). To visualize and evaluate the movement cycle trajectory for each condition combination, the normalized marker trajectories of the middle 30 movement cycles were averaged and plotted against cycle length. I also performed a similar procedure on the middle 30 segments from the respective top electrode EEG and bottom electrode EEG to visualize the two signals and look for any apparent trends or changes.

Statistical Analysis

I conducted statistical analysis using SPSS (version 29) and specified a significance level of 0.05. First, I calculated studentized residuals to detect the presence of any outliers in each data set. Outliers that were greater than ± 3 standard deviations from the mean of each data set were removed. I then assessed the assumptions of distribution normality and sphericity with Shapiro-Wilk's test and Mauchly's test, respectively. For any violations of the sphericity assumption, I applied the Greenhouse-Geisser correction to adjust the degrees of freedom for the subsequent analysis.

To evaluate the effects of waveform motion and testing setup on the generation of cable sway-induced motion artifact and whether or not they interact with each other, I conducted a two-way repeated measures analysis of variance (ANOVA) on each of the three outcome measures mentioned in the previous subsection (see Data Analysis, p. 8) after applying Z transformations, specifying waveform motion and testing setup as the within-subjects factors (Laerd Statistics, 2015). At each level of the analysis, I used the output p-values to interpret the results. I started by determining whether there was a statistically significant two-way interaction between the two factors. When a statistically significant two-way interaction was absent, I proceeded with

determining if there were any statistically significant main effects. Regardless of whether or not the main effects were found to be statistically significant, I proceeded with conducting a post hoc test on each main effect, specifically pairwise comparisons using the Bonferroni adjustment, and then concluded the analysis.

CHAPTER 3: RESULTS

Cable Sway and EEG Observations

Each of the non-normalized movement cycle trajectories in both testing setups exhibited full displacement magnitudes of approximately 20 mm (= 2 cm). In the Constrained setup, the magnitude of the difference between both peaks during the sinusoidal motion was 21.822 ± 0.003 mm, the magnitude of the difference between both peaks during the square motion was 21.807 ± 0.002 mm, and the magnitude of the peak during the sawtooth motion was 21.752 ± 0.005 mm. In the Unconstrained setup, the displacement magnitude during the sinusoidal motion was 19.361 ± 0.018 mm, the displacement magnitude during the square motion was 19.285 ± 0.004 mm, and the displacement magnitude during the sawtooth motion was 19.299 ± 0.016 mm (Fig. 6A, Fig. 7A). Additionally, the average signal amplitudes of the corresponding non-normalized top and bottom EEG signals appeared to randomly fluctuate between -0.5 and 0.5 μV, with respective standard deviations that appeared to be much greater in comparison, as shown by the sizes of the shaded regions encompassing the average signal amplitude lines (Fig. 6B, Fig. 7B).

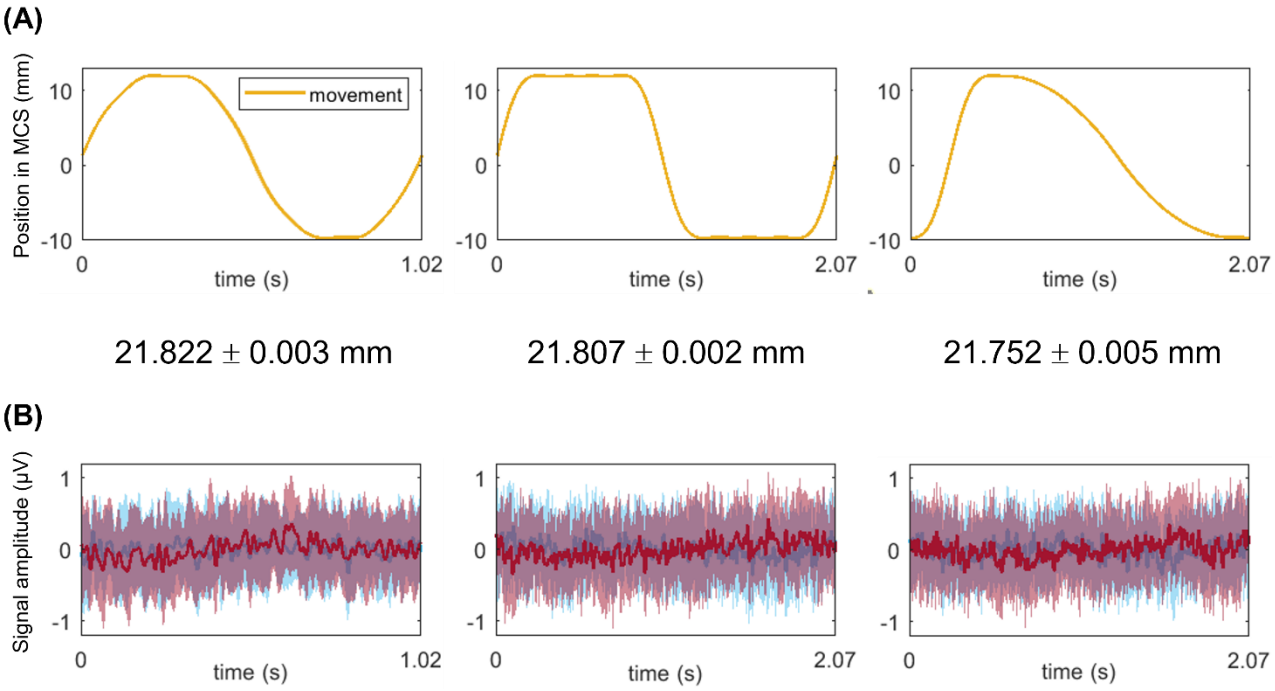

Figure 6: Non-normalized movement cycle trajectories and EEG signals resulting from controlled cable sway in Constrained setup. From left to right, (A) the movement cycle trajectory (in terms of position in the motion capture coordinate system (MCS)) and resulting full displacement magnitude (mean ± std) for the sinusoidal, square, and sawtooth motions, and (B) the top and bottom EEG signals corresponding to the sinusoidal, square, and sawtooth movement cycle trajectories. The blue line and surrounding shading represent the mean and standard deviation of the signal amplitude from the bottom electrode, while the red line and surrounding shading represent the mean and standard deviation of the signal amplitude from the top electrode.

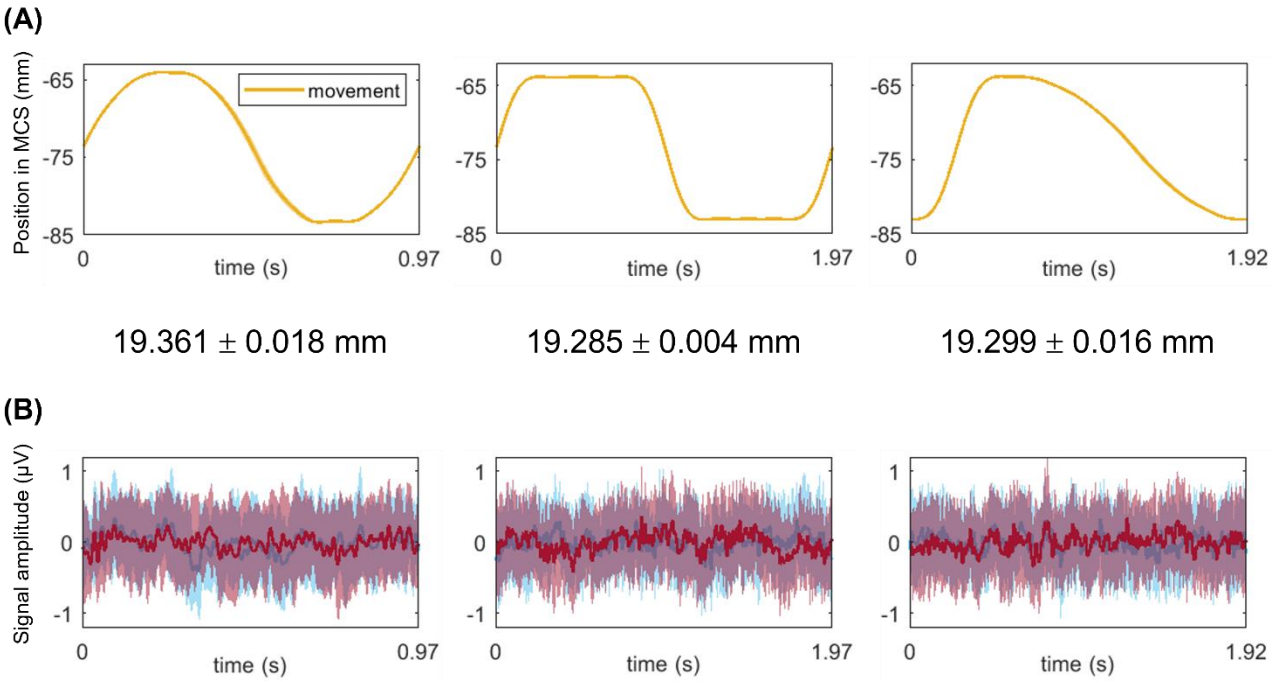

Figure 7: Non-normalized movement cycle trajectories and EEG signals resulting from controlled cable sway in Unconstrained setup. From left to right, (A) the movement cycle trajectory (in terms of position in the motion capture coordinate system (MCS)) and resulting full displacement magnitude (mean ± std) for the sinusoidal, square, and sawtooth motions, and (B) the top and bottom EEG signals corresponding to the sinusoidal, square, and sawtooth movement cycle trajectories. The blue line and surrounding shading represent the mean and standard deviation of the signal amplitude from the bottom electrode, while the red line and surrounding shading represent the mean and standard deviation of the signal amplitude from the top electrode.

With respect to shape, each resulting normalized movement cycle trajectory closely resembled the respective waveform programmed into the robotic arm to perform controlled motion, with slight differences in feature sharpness as compared to their ideal counterparts. The movement cycle trajectory produced by the square motion had rising and falling edges that were not instantaneous, as shown by their respective non-zero rise and fall times. The movement cycle trajectory produced by the sawtooth motion had a rising edge with a non-zero rise time and a negative ramp that was not linear (Fig. 4, Fig. 8A, Fig. 9A). Across all condition combinations, the normalized top and bottom EEG signals did not show any noticeable shapes or trends (Fig. 8B,

Fig. 9B). This was further reflected in the low correlation between top and bottom EEG (-0.005 ± 0.122, -0.012 ± 0.115, 0.027 ± 0.139 for sinusoidal, square, and sawtooth motions, respectively, in the Constrained setup; 0.017 ± 0.142, 0.008 ± 0.112, 0.030 ± 0.105 for sinusoidal, square, and sawtooth motions, respectively, in the Unconstrained setup), low correlation between cable sway and bottom EEG (-0.019 ± 0.256, 0.058 ± 0.238, -0.002 ± 0.208 for sinusoidal, square, and sawtooth motions, respectively, in the Constrained setup; 0.022 ± 0.281, 0.015 ± 0.190, -0.005 ± 0.216 for sinusoidal, square, and sawtooth motions, respectively, in the Unconstrained setup) and low correlation between cable sway and top EEG (-0.111 ± 0.313, -0.122 ± 0.223, -0.091 ± 0.281 for sinusoidal, square, and sawtooth motions, respectively, in the Constrained setup; 0.032 ± 0.261, 0.005 ± 0.198, -0.011 ± 0.278 for sinusoidal, square, and sawtooth motions, respectively, in the Unconstrained setup) (Fig. 8C - E, Fig. 9C - E).

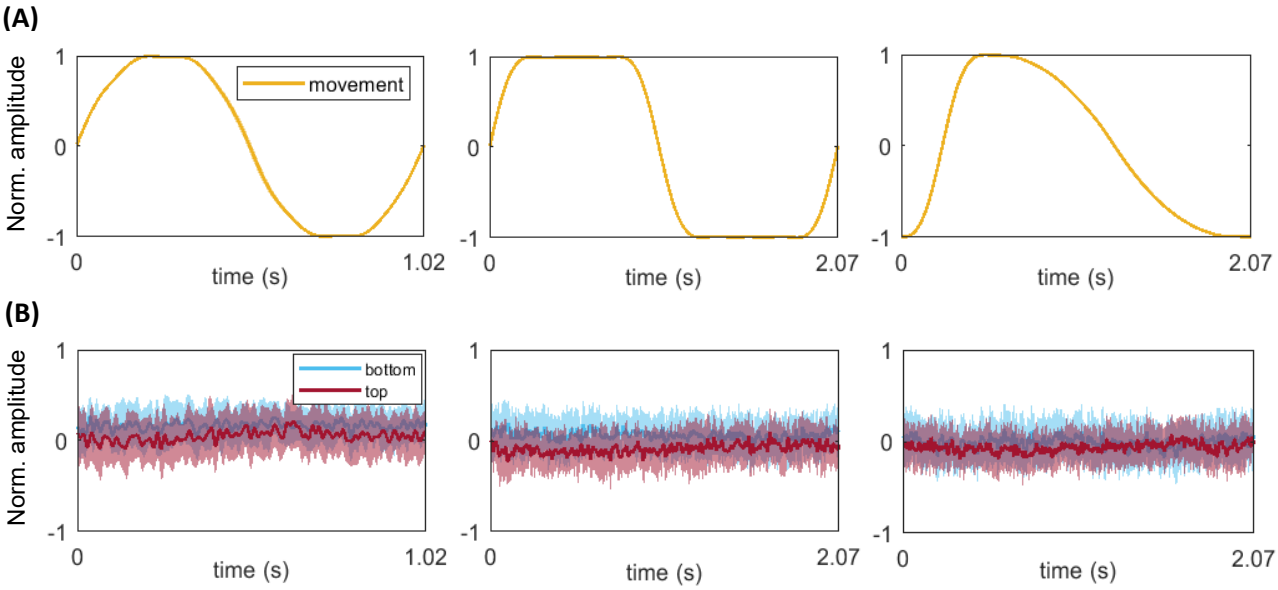

(C)

-0.005 ± 0.122 -0.012 ± 0.115 0.027 ± 0.139

(D)

-0.019 ± 0.256 0.058 ± 0.238 -0.002 ± 0.208

(E)

-0.111 ± 0.313 -0.122 ± 0.223 -0.091 ± 0.281

Figure 8: Normalized movement cycle trajectories and EEG signals resulting from controlled cable sway in Constrained setup. From left to right, (A) the movement cycle trajectory for the sinusoidal, square, and sawtooth motions, (B) the top and bottom EEG signals corresponding to the sinusoidal, square, and sawtooth movement cycle trajectories, (C) the Z-transformed correlation values (mean ± std) for the top and bottom EEG correlation outcome measure, (D) the Z-transformed correlation values (mean ± std) for the cable sway and bottom EEG correlation outcome measure, and (E) the Z-transformed correlation values (mean ± std) for the cable sway and top EEG correlation outcome measure.

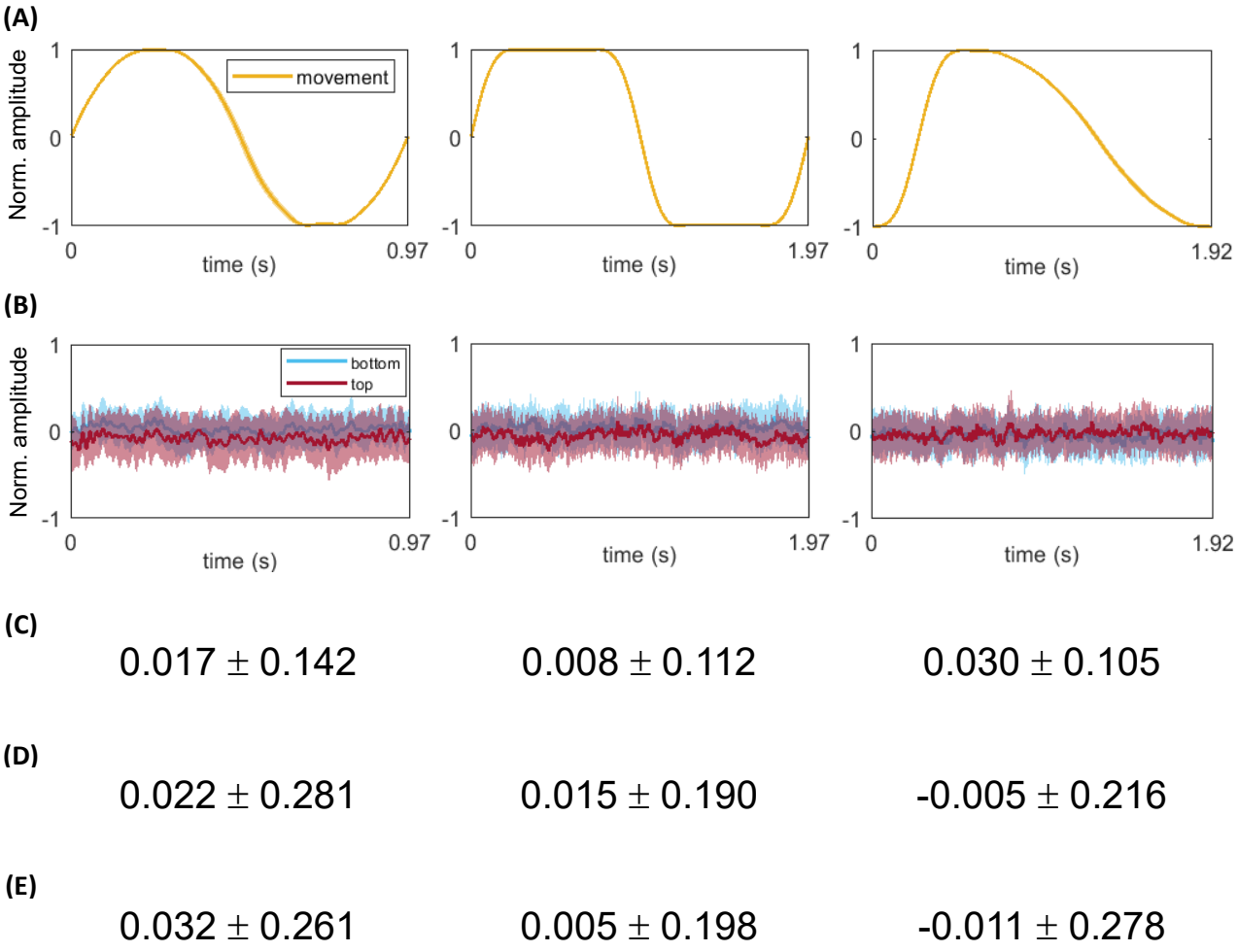

Figure 9: Normalized movement cycle trajectories and EEG signals resulting from controlled cable sway in Unconstrained setup. From left to right, (A) the movement cycle trajectory for the sinusoidal, square, and sawtooth motions, (B) the top and bottom EEG signals corresponding to the sinusoidal, square, and sawtooth movement cycle trajectories, (C) the Z-transformed correlation values (mean ± std) for the top and bottom EEG correlation outcome measure, (D) the Z-transformed correlation values (mean ± std) for the cable sway and bottom EEG correlation outcome measure, and (E) the Z-transformed correlation values (mean ± std) for the cable sway and top EEG correlation outcome measure.

Assumption Test Outcomes and Interaction Effects

No outliers were detected in any of the outcome measure data sets, as all studentized residuals were less than ±3 standard deviations from the mean of their respective data set. For the cable sway and bottom EEG correlation outcome measure, correlation values were normally distributed for all condition combinations (Shapiro-Wilk's test p's > 0.05). For the cable sway and

top EEG correlation outcome measure, correlation values were normally distributed for all condition combinations except sawtooth motion in the Unconstrained setup (Shapiro-Wilk's test $p = 0.021$), while for the top and bottom EEG correlation outcome measure, correlation values were normally distributed for all condition combinations except sawtooth motion in the Constrained setup (Shapiro-Wilk's test $p = 0.013$). Neither the cable sway and bottom EEG correlation outcome measure nor the cable sway and top EEG correlation outcome measure violated the assumption of sphericity (χ^2's = 0.363-5.162, p's > 0.05). However, the top and bottom EEG correlation outcome measure did violate the assumption of sphericity ($\chi^2 = 6.293$, $p = 0.043$), and a Greenhouse-Geisser correction was applied that estimated an epsilon (ε) value of 0.832. Waveform motion and testing setup did not have a statistically significant two-way interaction for any of the outcome measures (F's (2, 58) = 0.240-0.479, p's > 0.05; Greenhouse-Geisser corrected F (1.665, 48.282) = 0.119, p > 0.05).

Effects of Waveform Motion

Waveform motion did not have a statistically significant main effect for any of the outcome measures (F's (2, 58) = 0.083-0.954, p's > 0.05). This was further reflected by a lack of statistically significant differences between the mean correlations of the three waveform motions (pairwise comparison p's > 0.05) (Fig. 10).

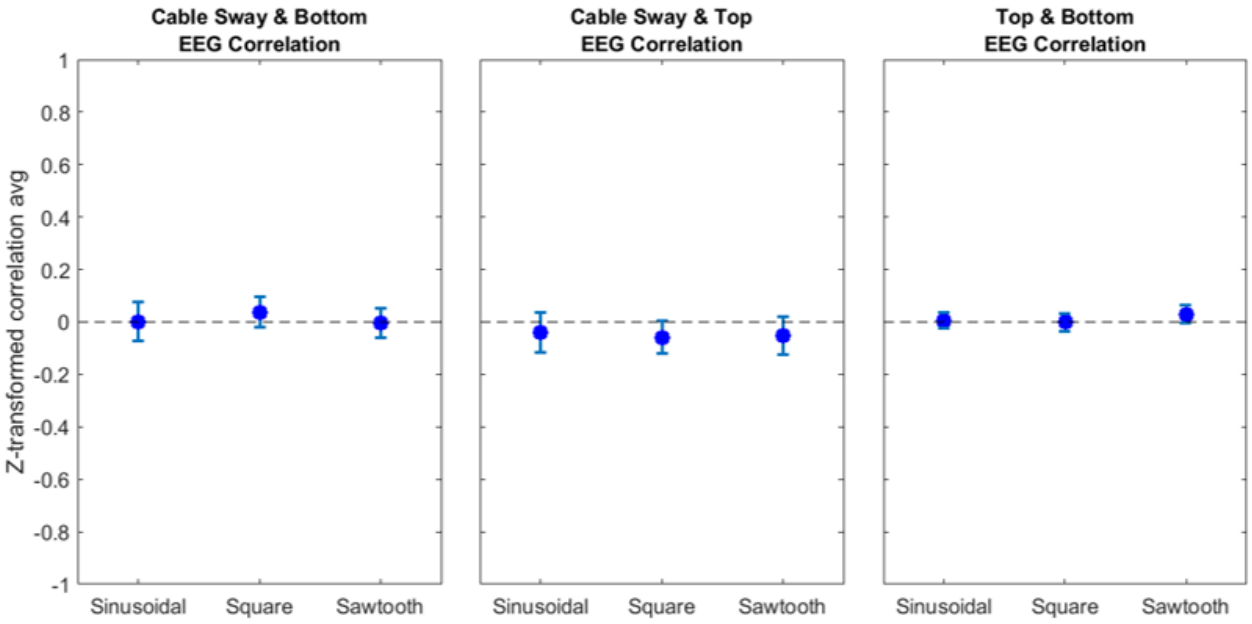

Figure 10: Average correlations between cable sway and bottom EEG, cable sway and top EEG, and top and bottom EEG during the sinusoidal, square, and sawtooth motions. Error bars represent the 95% confidence interval for each average. The differences in average correlation across the three waveform motions were not statistically significant for any of the outcome measures (p's > 0.05).

Effects of Testing Setup

For the cable sway and bottom EEG correlation outcome measure, as well as the top and bottom EEG correlation outcome measure, testing setup did not have a statistically significant main effect (F's (1, 29) = 0.003-0.615, p's > 0.05). As such, there was no statistically significant difference between the mean correlations of the two testing setups for either outcome measure (pairwise comparison p's > 0.05). However, for the cable sway and top EEG correlation outcome measure, testing setup did have a statistically significant main effect ($F(1, 29) = 9.323$, $p < 0.05$). Although not clearly apparent from a visual comparison, the difference between the mean correlations of the two testing setups was statistically significant (pairwise comparison $p < 0.05$) (Fig. 11).

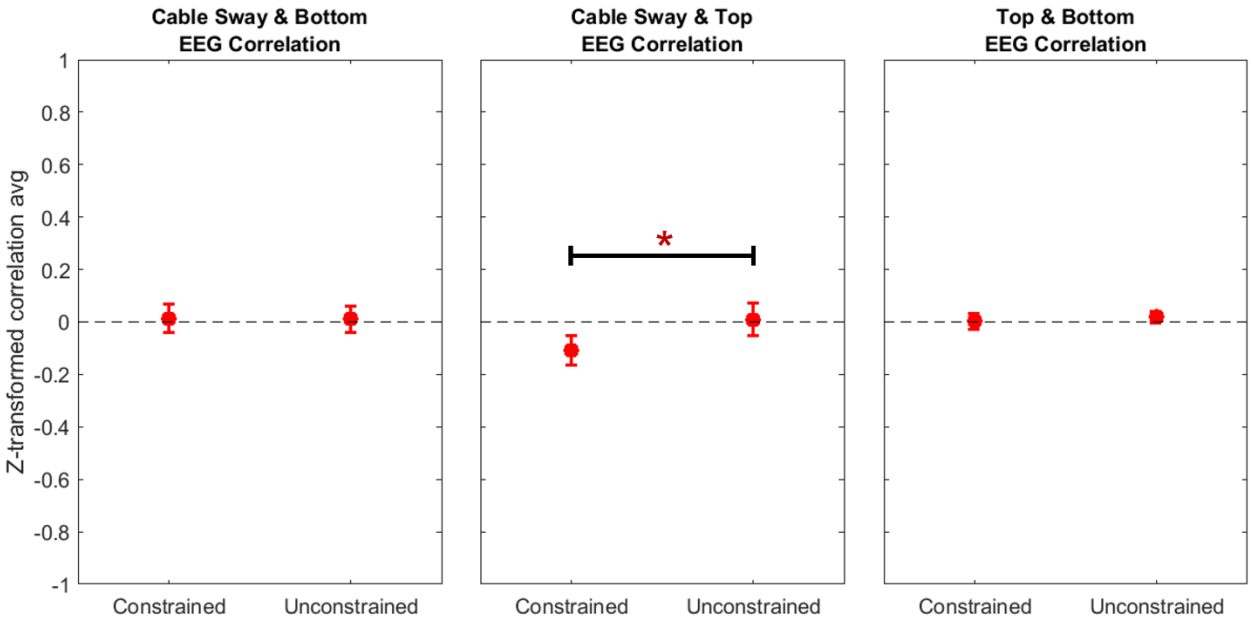

Figure 11: Average correlations between cable sway and bottom EEG, cable sway and top EEG, and top and bottom EEG in the Constrained and Unconstrained setups. Error bars represent the 95% confidence interval for each average. The difference in average correlation across the two setups was statistically significant for the cable sway and top EEG correlation outcome measure. The * symbol represents $p < 0.05$. The difference in average correlation across the two setups was not statistically significant for the cable sway and bottom EEG correlation outcome measure and the top and bottom EEG correlation outcome measure (p's > 0.05).

CHAPTER 4: DISCUSSION

I aimed to demonstrate that controlled cable sway in a benchtop setting could generate motion artifacts resembling specific waveforms in EEG signals collected with dual-sided electrodes. Cable sway and bottom EEG correlation, cable sway and top EEG correlation, and top and bottom EEG correlation randomly alternated from negative to positive across all waveform motions in both testing setups. Overall, the correlation outcome measures were low in magnitude for all controlled cable sway conditions.

Waveform motion did not affect the correlation between cable sway and bottom EEG, between cable sway and bottom EEG, or between top and bottom EEG. Additionally, the average cable sway and bottom EEG correlation, average cable sway and top EEG correlation, and average top and bottom EEG correlation were considerably low across all waveform motions irrespective of testing setup, deviating only slightly from zero. These results did not support our hypotheses that these three correlations would be high for each waveform motion.

Although unconstrained cable sway upstream of the electrodes – but not at the cable holder – was visually observed during each of the waveform motions in the Unconstrained setup, I inspected the EEG signal as it was recorded and did not notice any distinct shapes or trends reflective of motion artifacts. The average top and bottom EEG correlation in the Unconstrained setup was higher in magnitude than that in the Constrained setup. However, this difference was not statistically significant, indicating that the unconstrained cable sway produced in the Unconstrained setup did not do much to significantly increase correlation compared to constrained cable sway produced in the Constrained setup. Additionally, while the magnitude of the average cable sway and bottom EEG correlation was lower in the Unconstrained setup, this difference was

also not statistically significant. In contrast, a statistically significant difference was found in average cable sway and top EEG correlation, with lower magnitudes in the Unconstrained setup. Collectively, these results did not fully support the hypothesis that unconstrained cable sway would consistently yield lower correlation magnitudes compared to constrained cable sway across all outcome measures.

While this investigation did not yield many statistically significant results in terms of the outcome measures that I chose to evaluate, it is important to acknowledge its limitations. One limitation was the robotic arm, as it exhibited a tradeoff between displacement magnitude and movement frequency, such that for every increase in displacement magnitude there was a decrease in movement frequency. This made it difficult to perform the three different waveform motions at the same frequency and displacement magnitude. Consequently, I decided to control displacement magnitude only. I made this methodology decision prior to data collection with the expectation that the top and bottom EEG signals would resemble the specific waveforms programmed to produce controlled cable sway, similar to what has been observed in top and bottom EEG signals during controlled dual-sided electrode movement, where they closely resembled the sinusoidal motion programmed to move the electrodes in a couple of different directions (Li, 2022). Additionally, I expected that keeping the displacement magnitude consistent across the different waveforms would facilitate comparison of the corresponding EEG signals. While the frequency of electrode movement did have an effect on correlation between movement and the corresponding top and bottom EEG signals in the study performed by Li (2022), there was no visibly apparent pattern or trend in these correlations as frequency increased, so the strength of this effect remains unknown. Hence, for the purpose of this investigation, I assumed the frequency of controlled cable sway to have a negligible effect and instead prioritized displacement magnitude to focus more on

the signal waveforms that I expected to generate. Another limitation of this investigation was our use of conductive fabric to create a conductive interface with the electrodes. While conductive fabric was more practical for integration into our electrode holder, its electrical properties fail to mimic those of human skin (Li, 2022). Additional research may be needed that combines the dual conductive fabric layer approach with a material that more closely matches the electrical properties of human skin, such as ballistics gel, to allow benchtop studies of controlled cable sway to be more generalizable to human EEG (Owda & Casson, 2020).

It should be noted that for the cable sway and top EEG correlation outcome measure, the lack of a statistically significant two-way interaction between waveform motion and testing setup, waveform motion not having a statistically significant main effect, and testing setup having a statistically significant main effect were likely not attributed to correlation data that were not completely normally distributed across all unique condition combinations. I accepted this violation of distribution normality and ran the ANOVA to completion given that correlation data for five out of six condition combinations were still normally distributed and that repeated measures ANOVA is considered generally robust to normality as long as the sample size is at least 30 per condition, which in our case was equivalent to the middle 30 movement cycles and coinciding 30 segments of EEG data used to calculate 30 correlation values for each condition combination (Oberfeld & Franke, 2013). Additionally, for the top and bottom EEG correlation outcome measure, the lack of a statistically significant two-way interaction between waveform motion and testing setup, as well as neither waveform motion nor testing setup having a statistically significant main effect were likely not attributed to correlation data that were not completely normally distributed across all unique condition combinations or the violation of the sphericity assumption. I accepted the violation of distribution normality and ran the ANOVA to completion following the same rationale

as that for the cable sway and top EEG correlation outcome measure. Also, because Mauchly's test of sphericity is sensitive to deviations of normality, it was not surprising that the sphericity assumption was violated. However, our use of the Greenhouse-Geisser correction, which provides a more conservative measure of the extent of departure from sphericity, estimated an epsilon value that indicated that the violation of sphericity was not severe (Maxwell & Delaney, 2004; Oberfeld & Franke, 2013). Additionally, this adjustment produced F-statistics and p-values that were barely different from those produced without the adjustment, demonstrating that the violation of normality was minimal and supporting our decision to accept it.

Given the range of conditions under which I produced controlled cable sway, it is likely that the cables experienced varying degrees of mechanical deformation. Therefore, the findings of this investigation were unexpected considering that previous research has suggested that cable sway-induced motion artifact is generated by mechanical deformation and friction of the cables (Simakov & Webster, 2010; Symeonidou et al., 2018). However, the lack of significant findings does not necessarily reflect that controlled cable sway in a benchtop setting cannot produce specific motion artifacts resembling different waveforms. Although previous research has shown the generation of cable sway-induced motion artifact in conditions where controlled sinusoidal motion produced unconstrained cable sway, closer examination of the design of both of our testing setups revealed an interesting detail. As mentioned earlier in our methodology, I designed our electrode holder to minimize electrode movement relative to the conductive interface. However, previous studies did not appear to have sufficient controls for this specific movement. The instance of cable sway-induced motion artifact discussed by Webster (1984) was observed during human exercise, implying that the electrodes made contact with the skin, the latter of which deforms significantly during movement, inducing electrode movement even with good electrode-skin adhesion (Ershad

et al., 2023; Kim et al., 2022). While Symeonidou et al. (2018) used sports tape to secure the electrodes to the phantom head, the ballistics gel from which the head was made has a considerably low stiffness compared to the solid polylactic acid (PLA) that made up our electrode holder (Juliano et al., 2006; Vendland et al., 2019). Therefore, while the tape may have prevented the electrodes from being pulled out of the phantom head by the strain of the cables, it is likely that it did not prevent smaller electrode movements relative to their interface with the ballistics gel. In contrast, the higher stiffness of our electrode holder, combined with the tight fit of the electrodes in their wells and the relatively stationary well platforms, most likely contributed to eliminating electrode movement in all combinations of testing setup and waveform motion. According to Li (2022), controlled movement of dual-sided electrodes relative to a conductive interface can produce high correlation between top and bottom EEG, movement and top EEG, and movement and bottom EEG for different movement directions. Given that I replicated this conductive interface in our own investigation but made sure to eliminate electrode movement, our findings indicate that cable sway-induced motion artifact in EEG signals may arise not just from mechanical deformation of the cables, but also the simultaneous movement of the electrode itself, which alters the dynamics of the electrode-conductive surface interface.

LIST OF REFERENCES

Bertrand, A., Mihajlovic, V., Grundlehner, B., Van Hoof, C., & Moonen, M. (2013). Motion artifact reduction in EEG recordings using multi-channel contact impedance measurements. *2013 IEEE Biomedical Circuits and Systems Conference (BioCAS)*, 258–261.

Britton, J. W., Frey, L. C., & Hopp, J. L. (2016). Introduction. In E. K. St Louis & L. C. Frey (Eds.), *Electroencephalography (EEG): An introductory text and atlas of normal and abnormal findings in adults, children, and infants*. American Epilepsy Society.

Casson, A. J., Abdulaal, M., Dulabh, M., Kohli, S., Krachunov, S., & Trimble, E. (2018). Electroencephalogram. In T. Tamura & W. Chen (Eds.), *Seamless Healthcare Monitoring* (pp. 45–81). Springer International Publishing.

Ershad, F., Houston, M., Patel, S., Contreras, L., Koirala, B., Lu, Y., Rao, Z., Liu, Y., Dias, N., Haces-Garcia, A., Zhu, W., Zhang, Y., & Yu, C. (2023). Customizable, reconfigurable, and anatomically coordinated large-area, high-density electromyography from drawn-on-skin electrode arrays. *PNAS Nexus, 2*(1), pgac291.

Gwin, J. T., Gramann, K., Makeig, S., & Ferris, D. P. (2010). Removal of Movement Artifact From High-Density EEG Recorded During Walking and Running. *Journal of Neurophysiology*, *103*(6), 3526–3534.

Jacobsen, N. S. J., Blum, S., Scanlon, J. E. M., Witt, K., & Debener, S. (2022). Mobile electroencephalography captures differences of walking over even and uneven terrain but not of single and dual-task gait. *Frontiers in Sports and Active Living*, *4*, 945341.

Javaheri, S. H., Sepehri, M. M., & Teimourpour, B. (2014). Response Modeling in Direct Marketing. In *Data Mining Applications with R* (pp. 153–180). Elsevier.

Juliano, T. F., Forster, A. M., Drzal, P. L., Weerasooriya, T., Moy, P., & VanLandingham, M. R. (2006). Multiscale mechanical characterization of biomimetic physically associating gels. *Journal of Materials Research, 21*(8), 2084–2092.

Jungnickel, E., Gehrke, L., Klug, M., & Gramann, K. (2019). MoBI—Mobile Brain/Body Imaging. In *Neuroergonomics* (pp. 59–63). Elsevier.

Kim, H., Kim, E., Choi, C., & Yeo, W.-H. (2022). Advances in Soft and Dry Electrodes for Wearable Health Monitoring Devices. *Micromachines*, *13*(4), 629.

Kline, J. E., Huang, H. J., Snyder, K. L., & Ferris, D. P. (2015). Isolating gait-related movement artifacts in electroencephalography during human walking. *Journal of Neural Engineering*, *12*(4), 046022.

Laerd Statistics (2015). Two-way repeated measures ANOVA using SPSS Statistics. *Statistical tutorials and software guides.*

Li, J. (2022). *Electrode Evaluation and Electrocortical Dynamics of Adapting to Small Perturbations during Treadmill Walking* [Doctoral dissertation, University of Central Florida]. Electronic Theses and Dissertations, 2020-. https://purls.library.ucf.edu/go/DP0027098

Maxwell, S. E., & Delaney, H. D. (2004). *Designing experiments and analyzing data: A model comparison perspective* (2nd ed). Lawrence Erlbaum Associates.

Mihajlovic, V., Grundlehner, B., Vullers, R., & Penders, J. (2015). Wearable, Wireless EEG Solutions in Daily Life Applications: What are we Missing? *IEEE Journal of Biomedical and Health Informatics*, *19*(1), 6–21.

Mihajlovic, V., Patki, S., & Grundlehner, B. (2014). The impact of head movements on EEG and contact impedance: An adaptive filtering solution for motion artifact reduction. *2014 36th Annual International Conference of the IEEE Engineering in Medicine and Biology Society*, 5064–5067.

Nordin, A. D., Hairston, W. D., & Ferris, D. P. (2018). Dual-electrode motion artifact cancellation for mobile electroencephalography. *Journal of Neural Engineering*, *15*(5), 056024.

Oberfeld, D., & Franke, T. (2013). Evaluating the robustness of repeated measures analyses: The case of small sample sizes and nonnormal data. *Behavior Research Methods*, *45*(3), 792–812.

Oliveira, A. S., Schlink, B. R., Hairston, W. D., König, P., & Ferris, D. P. (2016). Induction and separation of motion artifacts in EEG data using a mobile phantom head device. *Journal of Neural Engineering*, *13*(3), 036014.

Owda, A. Y., & Casson, A. J. (2020). *Electrical properties, accuracy, and multi-day performance of gelatine phantoms for electrophysiology* [Preprint]. Bioengineering.

Richer, N., Downey, R. J., Hairston, W. D., Ferris, D. P., & Nordin, A. D. (2020). Motion and Muscle Artifact Removal Validation Using an Electrical Head Phantom, Robotic Motion Platform, and Dual Layer Mobile EEG. *IEEE Transactions on Neural Systems and Rehabilitation Engineering*, *28*(8), 1825–1835.

Simakov, A.B., & Webster, J.G. (2010). Motion Artifact from Electrodes and Cables. *Iranian Journal of Electrical and Computer Engineering (IJECE)*, *9*(2), 139-143. SID.

Singh, D., & Singh, B. (2020). Investigating the impact of data normalization on classification performance. *Applied Soft Computing*, *97*, 105524.

Symeonidou, E.-R., Nordin, A., Hairston, W., & Ferris, D. (2018). Effects of Cable Sway, Electrode Surface Area, and Electrode Mass on Electroencephalography Signal Quality during Motion. *Sensors*, *18*(4), 1073.

Vendland, L. E., Volkov-Muzylev, V. V., Demidov, A. N., & Borisov, Y. A. (2019). Room temperature testing of PLA plastics. *Journal of Physics: Conference Series*, *1359*(1), 012107.

Webster, J. G. (1984). Reducing Motion Artifacts and Interference in Biopotential Recording. *IEEE Transactions on Biomedical Engineering*, *BME-31*(12), 823–826.

Xu, J., Mitra, S., Van Hoof, C., Yazicioglu, R. F., & Makinwa, K. A. A. (2017). Active Electrodes for Wearable EEG Acquisition: Review and Electronics Design Methodology. *IEEE Reviews in Biomedical Engineering*, *10*, 187–198.